coatings

MDPI

Article

Development of Microstructured Carbon Coatings by Substrate-Catalytic CVD

Mattia Pierpaoli [1], Mirosław Sawczak [2] and Anna Dettlaff [3,*]

[1] Department of Metrology and Optoelectronics, Faculty of Electronics, Telecommunication and Informatics, Gdańsk University of Technology, 80-231 Gdańsk, Poland; matpierp@pg.edu.pl
[2] Institute of Fluid Flow Machinery, Polish Academy of Sciences, Fiszera 14, 80-231 Gdańsk, Poland; mireks@imp.gda.pl
[3] Department of Energy Conversion and Storage, Faculty of Chemistry, Gdańsk University of Technology, 11/12 Narutowicza St., 80-233 Gdansk, Poland
* Correspondence: anna.dettlaff@pg.edu.pl

Abstract: Carbon nanostructured films were synthesized by chemical vapor deposition (CVD) on H18 stainless steel (AISI 440C) sheets with an $H_2/CH_4/N_2$ gas mixture at various substrate temperatures. During the synthesis, the iron and chromium oxide layer was formed between the steel and carbonaceous layer. The carbon films exhibited wall-like and spherical morphologies and structures, as characterized by scanning electron microscopy and Raman spectroscopy. It was found that the synthesis temperature affects the microsphere density and, therefore, also in the electrochemical behavior. The electrochemical behavior of nanostructured carbon coatings strongly depends on the CVD deposition conditions. The best corrosion resistance (R_p = 11.8 MΩ·cm^2, I_{corr} = 4.4 nA·cm^{-2}) exhibits a nanostructured carbon sample with a moderate amount of sp^2-C-rich carbon microspheres CμSs synthesized at 700 °C. The corrosion resistance of the nanostructured carbon coating is better than raw stainless steel.

Keywords: carbon microspheres; chemical vapor deposition; corrosion resistance

Citation: Pierpaoli, M.; Sawczak, M.; Dettlaff, A. Development of Nanostructured Carbon Coatings by Substrate-Catalytic CVD. *Coatings* **2021**, *11*, 1403. https://doi.org/10.3390/coatings11111403

Academic Editor: Francesco Di Quarto

Received: 22 October 2021
Accepted: 15 November 2021
Published: 18 November 2021

1. Introduction

Nanostructured carbon coatings for steel electrodes, due to their remarkable characteristics, such as high electrical conductivity, hydrophobicity, and chemical inertness, have found a place in many applications as proton-exchange membrane fuel cells [1], porous current collectors for lithium-ion batteries [2], and as an effective support to grow carbon nanotubes [3–5], vertically-oriented graphene [6], carbon fibers [5] and micro-sized carbon spheres [5]. However, the coating properties can vary widely due to the substrate composition and synthesis conditions, for example, different qualities of the carbon layer can both support or worsen the substrate corrosion resistance. Diamond-like carbon coating, deposited after plasma nitriding, was found to enhance corrosion resistance [7], while carbon nanotubes and nanofibers, may accelerate intergranular corrosion, due to the chromium depletion of the near-surface steel region and chromium carbide precipitation at grain boundaries [8].

Recently, different carbon nanostructures on steel have been reported. Yuan et al. characterized the carbon created on the wall of a microwave plasma chemical vapor deposition (MPCVD) stainless steel substrate holder. The researchers found that high-quality 1- or 2–3-layer graphene sheets (GS) were formed [9] by using a CH_4/H_2 gas mixture at the temperature of ~500 °C and pressure of 30 Torr. Baddour et al. synthesized carbon nanotubes (CNTs) by thermal chemical vapor deposition (THCVD) directly on stainless steel (SS) substrates at 700 °C, using C_2H_2 and N_2 as the gas precursor and carrier, respectively [4], without the addition of external catalysts, since the iron in a commercial-grade

SS 304 acts as the catalyst itself. A double CNT layer was formed, nucleating in the island, characterized by a small diameter (5–20 nm, close to the substrate) widening to 40–70 nm and extending. Kurilich et al. synthesized CNTs on SS by microwave plasma enhanced chemical-vapor deposition (MPECVD), and they resolved the growth mechanism to the metal dusting process [3]. In another work, Lu et al. grew CNTs for corrosion resistance enhancement, finding that the corrosion current density of coated substrates can be decreased compared to the bare one [10]. Similarly, multi-walled carbon nanotubes (MWCNTs)were directly grown by CVD on as-received or pretreated 316 SS. N_2, H_2, and C_2H_4 were fed into the tube reactor preheated to a temperature of 760 °C. It was reported that the transition between CVD-grown nanotubes and nanofibers (CNFs) may occur due to the sample surface roughness [5]. Hashempour et al. [11] compared directly-grown CNTs on SS, focusing on the effect of the surface roughness. Since the diameters of CNTs are related to the catalyst particle size, larger nano-hills would favor the growth of thicker CNTs or, rather, CNFs. While CNFs can be considered a derivate form of CNTs, direct diamond growth on ferrous metals and those containing Ni or Co is challenging. The catalytic activity of these metals results in the formation of amorphous carbon instead of diamond. For this reason, while the deposition of an interlayer constitutes a viable but complex option to block the diffusion of metal catalyst particles toward the surface, direct deposition of diamond on steel can occur over a thick graphite interlayer, which results, however, in a worsening of the diamond film interface. Carbon diffusion into the steel also degrades the steel's properties; for this reason, decreasing the deposition temperature may help at the expense of the growth rate and diamond quality.

In this study, the surface of AISI440C stainless steel sheets was modified by chemical vapor deposition (CVD), forming a nanostructured carbon coating on the top. During the synthesis, the iron and chromium oxide layer was formed between the steel and carbonaceous layer. The effect of deposition temperature, which affects both the morphology, structure, and thereby on the electrochemical behavior of the carbon film-modified steel was investigated.

2. Materials and Methods

2.1. Sample Preparation

For the initial study on the effect of substrate roughness, stainless steel (AISI440C) squares of dimensions 20 mm × 20 mm × 0.5 mm were used as the substrates. Prior to the CVD process, the substrates were roughened by sandblasting and sonicated for 10 min in acetone, followed by isopropanol, and dried in nitrogen. Then, the samples were sonicated in a water-based nanodiamond slurry for 15 min and transferred to a CVD reactor. To investigate the temperature effect, the same procedure was adopted on cold-rolled steel samples with dimensions of 20 mm × 20 mm × 2 mm. The gas mixing ratio into CVD reactor was constant and equal to 100:8.3:1 (H_2:CH_4:N_2). The process duration of the carbon nanostructured coating (CNC) was equal to 5 h, microwave power set to 1300 W, and the substrate holder temperature was 500 °C (CNC-500 °C), 600°C (CNC-600 °C), and 700°C (CNC-700 °C). Further details on the process parameters can be found in our earlier work [12].

2.2. Sample Characterization

Scanning electron microscopy (Phenom XL using a 15 kV beam accelerating voltage, working in high vacuum mode, Thermo Fisher Scientific, Waltham, MA, USA) was used to observe the sample morphology and to study the elemental composition by energy dispersive X-ray analysis (EDX, Thermo Fisher Scientific). Image elaboration and processing were performed using the Gwyddion software (version 2.55). Graphical and statistical elaboration was performed in R and using the ggpubr package (version 0.1, 7.). The Raman spectra were acquired using a Raman microscope (InVia, Renishaw, New Mills, UK). Spectra were recorded over the range 200–3500 cm^{-1} with an integration time of 5 s (10

averages) using an argon-ion laser emitting at 514.5 nm (50× objective, grating 1800 l mm^{-1}) and operating at 5% of its total power of 50 mW.

The electrochemical evaluation was carried out using a VMP-300 potenti-ostat-galvanostat (BioLogic, Seyssinet-Pariset, France) in the EC-lab software (version V11.41). The studies were conducted in a three-electrode cell: Ag|AgCl served as the reference electrode (RE), a platinum wire as the counter electrode (CE), and the deposited nanostructured carbon was used as the working electrode (WE). The geometric area of the WE electrode was ca. 0.2 cm^2. The electrochemical properties of the nanostructured carbon coating were investigated using electrochemical impedance spectroscopy (EIS), and linear polarization (LP) techniques. EIS measurements were taken in the frequency range of 0.01 to 50,000 Hz (signal amplitude 10 mV; 6 points per frequency decade). Spectra were recorded at the rest potential ER. The EIS results were fitted using the ZSimpWin software (version V3.21). LP studies were performed in the polarization range between ± 0.25 V vs. E_R (scan rate = 1 $mV \cdot s^{-1}$). The LP results were fitted using TafelFit (EC-lab, version V11.41).

3. Results

3.1. Surface Morphology

3.1.1. Effect of the Stainless Steel Surface Roughness

Figure 1 shows the scanning electron microscopy (SEM) micrographs of bare as-received SS (a), after roughening by sandblasting (b), and after CVD growth in the as-received and sandblasted (c,d) states. According to Figure 1a,c nucleation occurs slower and within the boundary grains for the as-received SS. In contrast, for the roughed surface (Figure 1b,d), the growth occurs faster and more homogenously, making protruding grains barely distinguishable.

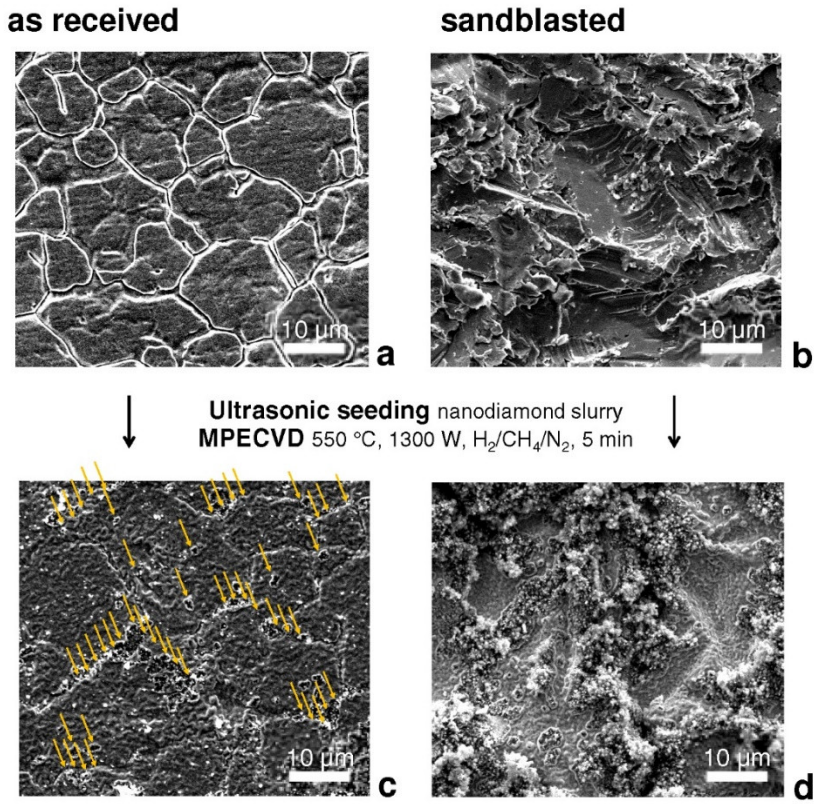

Figure 1. SEM micrographs of the bare SS surface (**a**) as received, (**b**) after surface roughening and (**c**,**d**) after CVD growth.

3.1.2. Effect of the CVD Process Duration

The growing process starts with the formation of amorphous carbon islands on the toughened edges of stainless steel (Figure 2a), which increase in extension (Figure 2b), covering the entire surface (Figure 2c). Moreover, after 30 min, part of the amorphous carbon vanishes, while carbon microspheres (CμSs) appear, with diameters of a few micrometers.

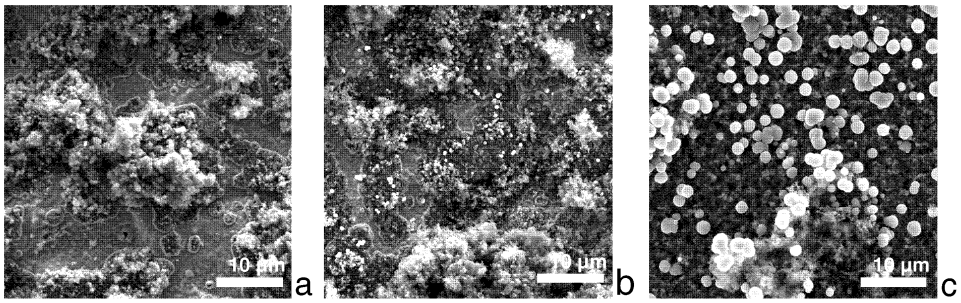

Figure 2. CμSs growth mechanism. Deposition time: (**a**) 5 min, (**b**) 15 min and (**c**) 30 min.

3.1.3. Effect of the Temperature During CVD

The substrate holder temperature in the CVD chamber was varied, and the effect was investigated. In Figure 3, SEM micrographs are shown. As can be seen with decreasing synthesis temperature, there is an increase in the superficial density of the CuSs grown on nanostructured carbon which tends to accumulate into larger clusters. The phenomena can be seen most of all for CNC-500 °C samples.

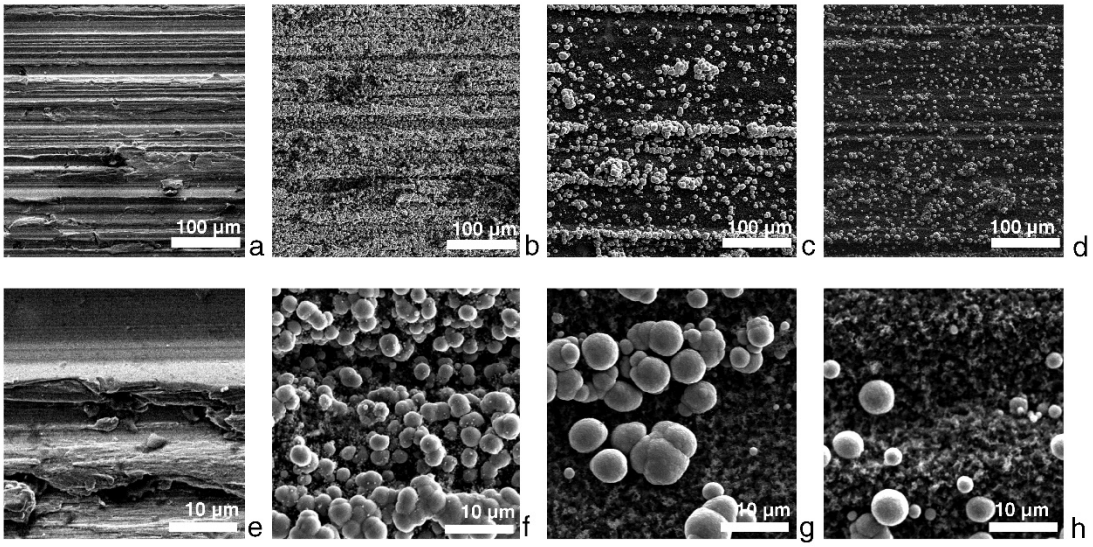

Figure 3. Effect of the temperature used during CVD process: (**a**,**e**) SS as provided, at (**b**,**f**) 500 °C, (**c**,**g**) 600 °C, (**d**,**h**) 700 °C.

Figure 4 reports the Raman spectra of the samples after CVD growth at different temperatures. The characteristic peak of the G band is located at 1581 ± 1 cm^{-1} and indicates the presence of crystalline hexagonal graphite (i.e., sp^2-C). The characteristic peak of the D band is located at ~1356 cm^{-1} and arises due to a disorder-induced phonon mode, indicating the presence of disorders in the carbon nanostructures. The D and D′ peaks require a defect for their activation in the double resonance Raman scattering. The 2D peak is strongly dispersive with excitation energy and is activated by triple resonance Raman scattering, as well as for the 2D′ peak, which is the second-order of the intra-valley D′ peak [13]. In order to compare quantitatively the different peak features, results of the peak fitting procedure are reported in Table 1.

Table 1. Results of the Raman spectra fitting.

Band	D		G		D′		2D		D+D′		–	–
Temp	xc	FWHM	xc	FWHM	xc	FWHM	xc	FWHM	xc	FWHM	I_D/I_G	$I_D/I_{D'}$
500	1354.2	40.4	1582.8	32.0	1620.3	20.0	2706.3	58.9	2944.6	70.9	1.18	5.8
600	1356.1	27.8	1581.3	16.6	1622.9	6.7	2708.6	42.0	2968.0	34.9	0.43	4.0
700	1353.0	30.0	1580.8	17.9	1622.0	9.3	2710.8	46.4	2948.7	60.0	0.47	4.5
CμS	1335.2	158.4	1578.8	62.0	1620.0	27.3	2708.2	227.4	2903.0	248.6	1.46	4.8

The I (D)/I (G) ratio is almost halved for the high-temperature deposition, in comparison to the CNC-500 °C sample. Interestingly, the latter is comparable to the CμS one; this is probably due to the high density of microspheres. The decrease in the I (D)/I (G) ratio with the growing temperature suggests the ordering of the graphitic structure [14,15]. Moreover, the similar I (D)/I (D′) ratio for all of the samples is equal to 4.6 ± 0.6, which suggests that the presence of edge defect is predominant. The decrease in the D′ intensity and the full width at half maximum (FWHM) of the G peak, with the increasing deposition temperature, is consistent with our previous study [16]. The 2D peak shape is comparable between the different samples (as also reported by the similar FWHM), while its area decreases with increasing temperature. Similarly, the intensities of the D + D′ peak for the samples grown at higher temperatures are lower than the CNC-500 °C sample.

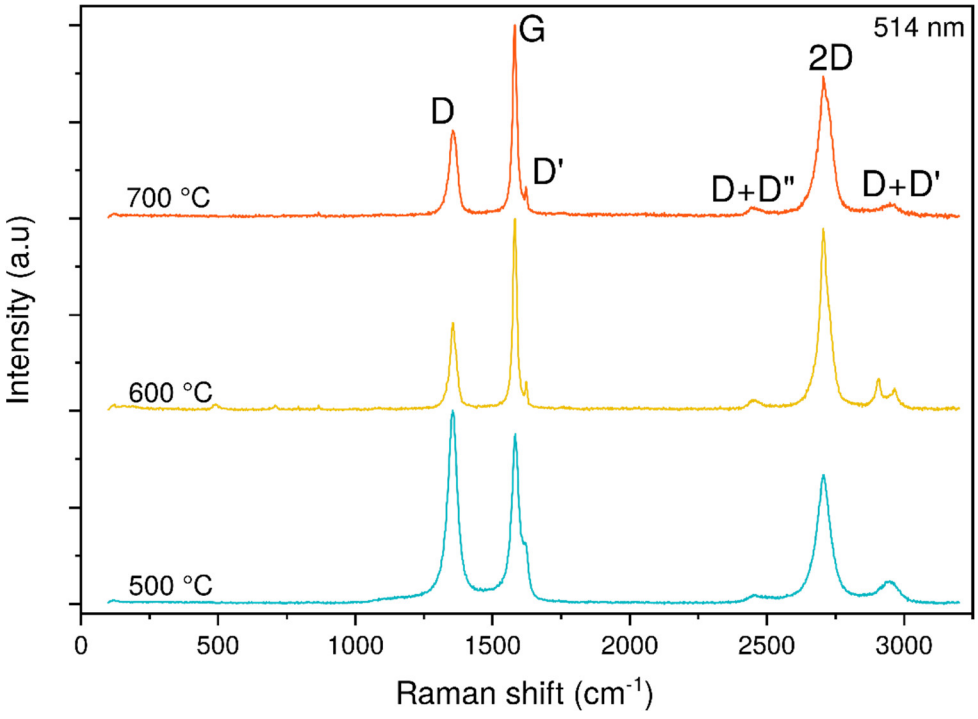

Figure 4. Raman spectra of the carbon coating layer after CVD at 500, 600, and 700 °C.

EDX analysis of the sample cross-sections revealed the presence of C, Fe, Cr, Ni, and O at variable percentages across the substrate depth. The raw steel sample has a composition of Fe (~46 at.%), O (~22 at.%), Ni (~17 at.%), Cr (~13 at.%), C (~1 at.%) and Si (~1 at.%). From Figure 5, it is possible to observe that, after the CVD process, the upper part of the steel substrate (with a thickness of ~200 µm) is enriched with C (up to ~85 at.%), followed by a layer rich in Fe and Cr oxides. The bottom of the sample, which has not been exposed to the plasma, but only to the thermal treatment, exhibits an interface rich in Fe and Cr.

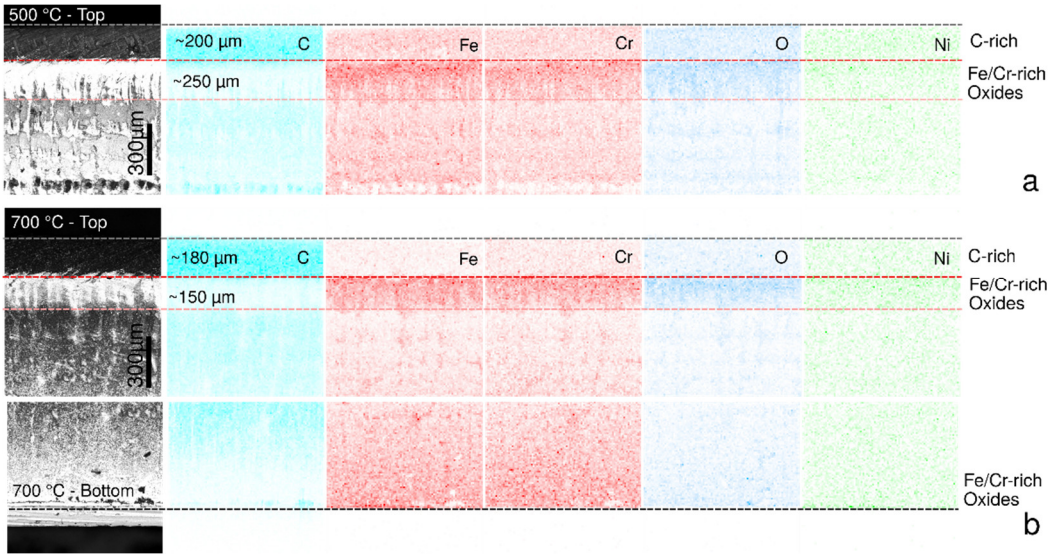

Figure 5. EDX of sample cross-sections deposited at (**a**) 500 °C and (**b**) 700 °C.

During the CVD process, two processes occur simultaneously: the formation of irregular, highly porous, carbon-rich microstructure, and the nucleation of carbon spheres with a diameter of a few micrometers (Figure 6a). Both spectra show typical features of graphitic films characterized by the presence of G, D, D′, 2D,D + D″,D + D′ peaks; however, the CµSs also exhibits a shoulder peak at ≈ 1120 cm^{-1}, which can be attributed to the D″ band. The CµSs Raman spectra present increased FWHM, pointing to an increased content of sp^2-hybridized carbon compared to the underlying C-layer.

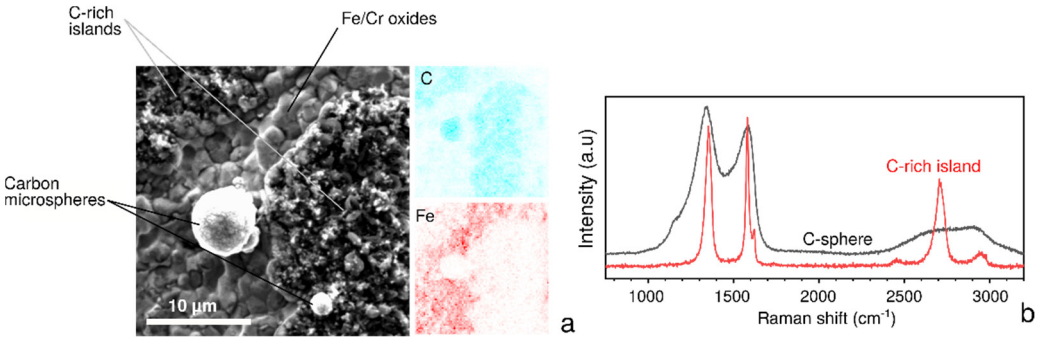

Figure 6. (**a**) SEM micrograph and EDX mapping of the C and Fe elemental composition. (**b**) Raman spectra of the two different C-rich regions identified in the SEM image.

The CμSs density increases with the decreasing CVD synthesis temperature. At 500 °C, the substrate appears almost entirely covered by the CμSs, which stack together. At higher temperatures, smaller clusters are present; however, it is still possible to distinguish them separately. For these reasons, it is difficult to estimate the particle density of the 500 °C samples, but it is still possible to find a hundredfold increase compared to the sample obtained at the highest temperature (Figure 7a). Similarly, no significant difference in the diameters of the CμSs was found for the samples grown at a temperature equal to or greater than 600 °C (Figure 7b). A few hypotheses have been postulated to explain the growth mechanism of such spheres. Ni and Fe are known catalysts for CVD growth of carbon nanotubes or other carbon nanostructures [17], and it is possible to observe a few such filamentous structures (Figure 7c, in orange). However, the formation of catalysts chunks, which cannot catalyze CNTs growth, may lead to further coating by amorphous carbon [18] (Figure 7c, in yellow). Then, the amorphous carbon grows preferably in clusters, increasing in size until carbon spheres are formed. Increasing temperature enhances carbon diffusion through the upper layer of the steel substrate (Figure 7c, in purple); for this reason, the formation of amorphous carbon, thus carbon microsphere, is inhibited.

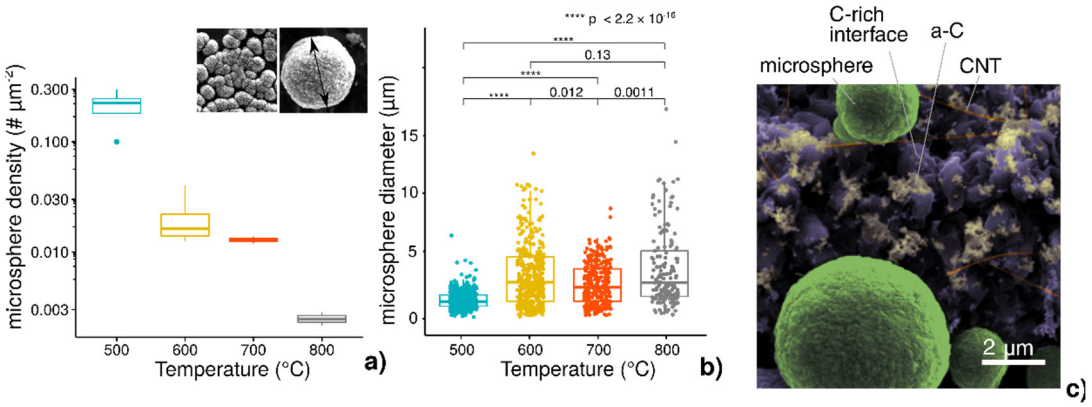

Figure 7. Carbon microsphere (**a**) density, (**b**) average diameter for the different temperatures, (**c**) colored SEM image.

3.2. Electrochemical Characterization

The surface resistance of the nanostructured carbon was investigated in synthetic domestic wastewater (detailed composition can be found elsewhere [19]) using the EIS and LP techniques. The results are shown in Figure 8a–b. In order to better understand the electrochemical characteristics of the test samples, an electrical equivalent circuit (EEC) was used to analyze the EIS results. In the EEC, R_1 corresponds to the solution resistance, R_2 is coating resistance, C_2 is the coating capacitance, R_3 is the charge transfer resistance, and CPE_3 is the constant phase element. CPE_3 is defined as $Z_{CPE3} = [Q_3(j\omega)^{n3}]^{-1}$, where Q_3 is a proportional factor, ω reflects the angular frequency, j is the imaginary number, and n_3 corresponds to the constant rate element parameter describing, inter alia, the homogeneity of the layer and non-uniform distribution of the current. The presented electrical equivalent circuit is represented by two time constants {R_2, C_2} and {R_3, Q_3}, respectively. The first time constant (τ_2) may refer to the carbon layer, while the second time constant (τ_3) may be related to the charge transfer process at the electrode interphase. The values of estimated electrical elements are gathered in Table 2.

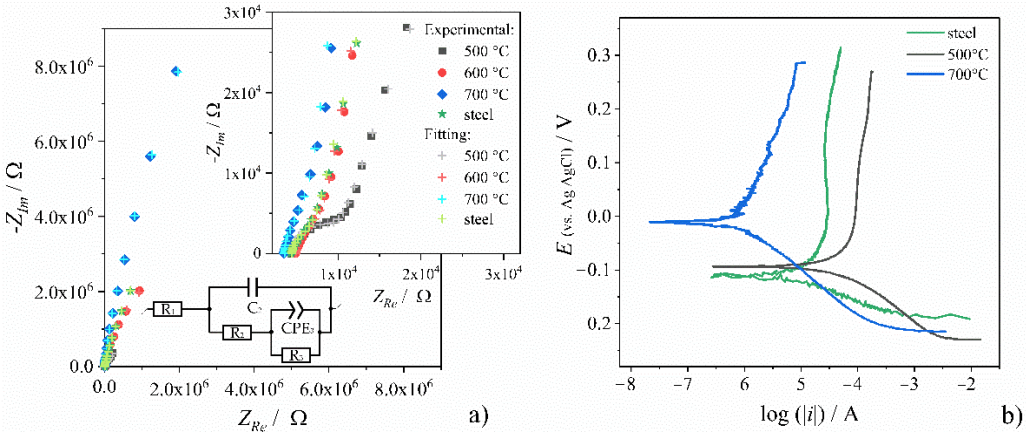

Figure 8. (**a**) Nyquist representation of electrochemical impedance spectra, and (**b**) linear polarization curves recorded on chosen nanostructured carbon electrodes immersed in synthetic domestic wastewater.

Table 2. Selected parameters calculated on the basis of the EEC.

Parameter	SS	CNC-500 °C	CNC-600 °C	CNC-700 °C
C_2/μF·cm^{-2}	5.9	7.8	8.2	3.9
R_2/Ω·cm^2	926	1216	1314	2117
Q_3/Ω^{-1}·cm^{-2} s^n	2.7 × 10^{-5}	1.1 × 10^{-4}	2.5 × 10^{-5}	6.3 × 10^{-6}
n_3	0.84	0.79	0.87	0.89
R_3/Ω·cm^2	3.61 × 10^6	3.33 × 10^5	1.50 × 10^6	1.18 × 10^7

The polarization resistance (R_p) is inversely proportional to the corrosion rate and is a sum of the coating resistance and charge transfer resistance [19,20]. The value of R_p increase with the growing CVD synthesis temperature. For the coating obtained at t = 700 °C, the polarization resistance is higher than the value achieved for the raw steel (3.61 MΩ·cm^2) and it is equal to 11.8 MΩ·cm^2. Furthermore, with the increasing temperature of the sample preparation, an increase in the parameter n can be observed, which indicates an increase in the level of surface electric homogeneity of the carbon layers.

Linear polarization was also conducted in synthetic domestic wastewater. The corrosion potential and current density values are collected in Table 3. The highest corrosion potential, equal to −11.9 mV, was recorded for the sample synthesized at the highest temperature 700 °C. The same sample is characterized by the lowest corrosion current of 4.4 nA·cm^{-2}. The raw steel shows a ten times higher corrosion current equal to 40.8 nA·cm^{-2}, and the lowest E_{corr} (−115.6 mV).

Table 3. Results of linear polarization tests.

Parameter	SS	CNC-500 °C	CNC-700 °C
E_{corr}/mV	−115.6	−104.6	−11.9
$I_{corr}/nA{\cdot}cm^{-2}$	40.8	361.8	4.4
β_a/mV	151.0	1151.4	272.7
β_c/mV	39.2	79.50	83.4

4. Discussion

The growth of carbon coating is enhanced by sandblasting the stainless-steel surface, while for the untreated sample, carbon nanostructures are formed between the stainless-steel microstructure grains boundaries (Figure 1). The reason for the faster graphitic carbon growth eased by the roughened surface may arise from the locally enhanced plasma, which induces surface and interface defects, favoring an irregular nanostructure growth.

The formation of CμSs is affected mainly by two factors: firstly, they preferably grow close to carbon-rich non-catalytic sites, which are easily covered by amorphous carbon, acting as a carbon buffering layer [21] and, secondly, high temperatures inhibit their formation. Nevertheless, the reason behind their nucleation and growth is still debated. Ghaemi et al. attribute their formation to the Fe catalyst, characterized by a diameter of 100–200 nm [22]. Iron does indeed have a catalytic behavior toward sp^2-C formation, and carbon possesses high diffusivity toward this metal. Singhal et al. reported that Fe, as a catalyst, plays an essential role in forming carbon nanotubes. In contrast, CμSs are synthesized directly by a mixture of xylene and benzene, at 900 °C, in the absence of a catalyst [23].

Similarly, Chen et al. pointed out the formation of CμSs with diameters between 500 nm and 3 μm as a consequence of the high C_2H_2:H_2 ratio (using an AISI 304 SS as the substrate) [2]. On the other hand, Shu et al. described that the formation of CμSs assemblies is due to the growth rate of the carbon layer, which exceeds the migration rate of metal atoms (from the substrate to the surface), which would otherwise catalyze the formation of filament [1]. However, while in the study mentioned above, the increase in temperature favors particle formation, in the present one, the increase in temperature hampers the formation of the CμSs. At lower temperatures, the steel substrates work as a catalyst, due to the limited carbon diffusion into the steel (Figure 3 + EDX cross-section), favoring the rapid development of micrometer-sized sp^2-C-rich CμSs. Moreover, at the lowest temperature (500 °C), the sphere growth is so fast that they tend to agglomerate into bigger clusters.

According to the EIS and LP results, the amount of the carbon microspheres strongly influence electrochemical performance. The carbon coating deposited at 500°C shows high surface electric heterogeneity (n_3 = 0.79), which may be related to the agglomeration of the carbon microspheres. The CNC-500 °C sample also shows the highest corrosion current possibly resulting from the low adhesion of the agglomerated spheres. The carbon coatings synthesized at higher temperatures are characterized by a smaller number of microspheres. The surface of CNC-600 °C and CNC-700 °C exhibit higher surficial homogeneity. The CμSs are less agglomerated and thus probably they are better attached to the carbon matrix. As a result, the CNC-700 °C sample exhibits good corrosion resistance in synthetic domestic leachates.

5. Conclusions

In this study, nanostructured carbon coatings were deposited on AISI440C steel using chemical vapor deposition. During the synthesis process, two processes occur simultaneously: the formation of irregular, highly porous, carbon-rich microstructures and the nucleation of carbon spheres with a diameter of a few micrometers. During the synthesis between the steel and carbon coating, the iron and chromium oxide layer was created.

The formation of carbon microspheres CμSs is affected mainly by two factors: firstly, they preferably grow close to carbon-rich non-catalytic sites, which are easily covered by amorphous carbon, acting as a carbon buffering layer and, secondly, high temperatures inhibit their formation.

The electrochemical behavior of nanostructured carbon coatings strongly depends on the CVD deposition conditions. The best corrosion resistance (R_p = 11.8 MΩ·cm^2, I_{corr} = 4.4 nA cm^{-2}) exhibits a nanostructured carbon sample with a moderate amount of sp^2-C-rich CμSs synthesized at 700 °C (the corrosion resistance is better than raw stainless steel).

Author Contributions: Conceptualization, M.P.; methodology, M.P.; formal analysis, M.P. and A.D.; investigation, M.P. and M.S.; resources, M.S.; writing—original draft preparation, M.P. and A.D.; writing—review and editing, A.D.; visualization,M.P. and A.D. project administration, M.P. All authors have read and agreed to the published version of the manuscript.

Funding: This research was supported by the Polish National Agency for Academic Exchange (NAWA), under the Ulam program (Grant No. PPN/ULM/2019/1/00061/DEC/1) (M. Pierpaoli). Financial support of COE'2020 conference within the framework of the Excellent Science (Doskonała Nauka, DNK/SP/462114/2020) project of Polish Ministry of Education and Science, MEN is acknowledged.

Institutional Review Board Statement: Not applicable.

Informed Consent Statement: Not applicable.

Data Availability Statement: Data sharing is not applicable to this article.

Conflicts of Interest: The authors declare no conflicts of interest.

References

1. Shu, S.; Dai, D.; Chung, C.Y.; Yuan, Q.; Wang, B.; Hung, T.T.; Dai, W.; Wei, Q.; Fu, L.; Yu, J.; et al. Significant enhancement of corrosion resistance of stainless steel with nanostructured carbon coatings by substrate-catalytic CVD. *Appl. Nanosci.* **2021**, *11*, 725–733, doi:10.1007/s13204-020-01621-6.
2. Chen, S.K.; Chiu, K.F.; Su, S.H.; Liu, S.H.; Hou, K.H.; Leu, H.J.; Hsiao, C.C. Low contact resistance carbon thin film modified current collectors for lithium Ion batteries. *Thin Solid Films.* **2014**, *572*, 56–60, doi:10.1016/j.tsf.2014.07.064.
3. Kurilich, M.R.; Thapa, A.; Moilanen, A.; Miller, J.L.; Li, W.; Neupane, S. Comparative study of electron field emission from randomly-oriented and vertically-aligned carbon nanotubes synthesized on stainless steel substrates. *J. Vac. Sci. Technol. B.* **2019**, *37*, 041202, doi:10.1116/1.5098782.
4. Baddour, C.E.; Fadlallah, F.; Nasuhoglu, D.; Mitra, R.; Vandsburger, L.; Meunier, J.L. A simple thermal CVD method for carbon nanotube synthesis on stainless steel 304 without the addition of an external catalyst. *Carbon.* **2009**, *47*, 313–318, doi:10.1016/j.carbon.2008.10.038.
5. Kruehong, S.; Kruehong, C.; Artnaseaw, A. Branched carbon fibres and other carbon nanomaterials grown directly from 304 stainless steel using a chemical vapour deposition process. *Diam. Relat. Mater.* **2016**, *64*, 143–152, doi:10.1016/j.diamond.2016.02.011.
6. Rozel, P.; Radziuk, D.; Mikhnavets, L.; Khokhlov, E.; Shiripov, V.; Matolínová, I.; Matolín, V.; Basaev, A.; Kargin, N.; Labunov, V. Properties of nitrogen/silicon doped vertically oriented graphene produced by ICP CVD Roll-to-roll technology. *Coatings.* **2019**, *9*, 1–24, doi:10.3390/coatings9010060.
7. Fenili, C.P.; de Souza, F.S.; Marin, G.; Probst, S.M.H.; Binder, C.; Klein, A.N. Corrosion resistance of low-carbon steel modified by plasma nitriding and diamond-like carbon. *Diam. Relat. Mater.* **2017**, *80*, 153–161, doi:10.1016/j.diamond.2017.11.001.
8. Hashempour, M.; Vicenzo, A.; Zhao, F.; Bestetti, M. Effects of CVD direct growth of carbon nanotubes and nanofibers on microstructure and electrochemical corrosion behavior of 316 stainless steel. *Mater. Charact.* **2014**, *92*, 64–76, doi:10.1016/j.matchar.2014.03.001.
9. Yuan, G.D.; Zhang, W.J.; Yang, Y.; Tang, Y.B.; Li, Y.Q.; Wang, J.X.; Meng, X.M.; He, Z.B.; Wu, C.M.L.; Bello, I.; et al. Graphene sheets via microwave chemical vapor deposition. *Chem. Phys. Lett.* **2009**, *467*, 361–364, doi:10.1016/j.cplett.2008.11.059.
10. Lu, C.; Shi, F.; Jin, J.; Peng, X. Study on the properties of vertical carbon nanotube films grown on stainless steel bipolar plates. *Materials.* **2019**, *16*, 899, doi:10.3390/ma12060899.
11. Hashempour, M.; Vicenzo, A.; Zhao, F.; Bestetti, M. Direct growth of MWCNTs on 316 stainless steel by chemical vapor deposition: Effect of surface nano-features on CNT growth and structure. *Carbon.* **2013**, *63*, 330–347, doi:10.1016/j.carbon.2013.06.087.
12. Pierpaoli, M.; Jakobczyk, P.; Sawczak, M.; Łuczkiewicz, A.; Fudala-Książek, S.; Bogdanowicz, R. Carbon nanoarchitectures as high-performance electrodes for the electrochemical oxidation of landfill leachate. *J. Hazard. Mater.* **2021**, *401*, 123407, doi:10.1016/j.jhazmat.2020.123407.
13. Ferrari, A.C.; Basko, D.M. Raman spectroscopy as a versatile tool for studying the properties of graphene. *Nat. Nanotechnol.* **2013**, *8*, 235–246, doi:10.1038/nnano.2013.46.
14. Pierpaoli, M.; Ficek, M.; Jakobczyk, P.; Karczewski, J.; Bogdanowicz, R. Self-assembly of vertically oriented graphene nanostructures: Multivariate characterization by Minkowski functionals and fractal geometry. *Acta Mater.* **2021**, 116989, doi:10.1016/j.actamat.2021.116989.
15. Dettlaff, A.; Das, P.R.; Komsiyska, L.; Osters, O.; Łuczak, J.; Wilamowska-Zawłocka, M. Electrode materials for electrochemical capacitors based on poly(3,4 ethylenedioxythiophene) and functionalized multi-walled carbon nanotubes characterized in aqueous and aprotic electrolytes. *Synth. Met.* **2018**, *244*, 80–91, doi:10.1016/j.synthmet.2018.07.006.
16. Pierpaoli, M.; Ficek, M.; Rycewicz, M.; Sawczak, M.; Karczewski, J.; Ruello, M.; Bogdanowicz, R. Tailoring electro/optical properties of transparent boron-doped carbon nanowalls grown on quartz. *Materials.* **2019**, *12*, 547, doi:10.3390/ma12030547.

17. Hata, K.; Futaba, D.N.; Mizuno, K.; Namai, T.; Yumura, M.; Iijima, S. Water-assisted highly efficient synthesis of impurity-free single-walled carbon nanotubes. *Science.* **2004**, *306*, 1362–1364, doi:10.1126/science.1104962.
18. Kumar, A.; Kostikov, Y.; Orberger, B.; Nessim, G.D.; Mariotto, G. Natural laterite as a catalyst source for the growth of carbon nanotubes and nanospheres. *ACS Appl. Nano Mater.* **2018**, *1*, 6046–6054, doi: 10.1021/acsanm.8b01117.
19. Dettlaff, A.; Brodowski, M.; Kowalski, M.; Stranak, V.; Prysiazhnyi, V.; Klugmann-Radziemska, E.; Ryl, J.; Bogdanowicz, R. Highly oriented zirconium nitride and oxynitride coatings deposited via high-power impulse magnetron sputtering: Crystal-facet-driven corrosion behavior in domestic wastewater. *Adv. Eng. Mater.* **2021**, *23*, 2001349, doi:10.1002/adem.202001349.
20. Liu, W.; Zhou, Q.; Li, L.; Wu, Z.; Cao, F.; Gao, Z. Effect of alloy element on corrosion behavior of the huge crude oil storage tank steel in seawater. *J. Alloys Compd.* **2014**, *598*, 198–204, doi:10.1016/j.jallcom.2014.01.181.
21. Vander Wal, R.L.; Hall, L.J. Carbon nanotube synthesis upon stainless steel meshes. *Carbon.* **2003**, *41*, 659–672, doi:10.1016/S0008-6223(02)00369-X.
22. Ghaemi, F.; Yunus, R.; Mohd Salleh, M.A.; Lim, H.N.; Rashid, S.A. Bulk production of high-purity carbon nanosphere by combination of chemical vapor deposition methods. *Fullerenes Nanotub. Carbon Nanostruct.* **2015**, *23*, 669–675, doi:10.1080/1536383X.2014.951439.
23. Singhal, S.; Dixit, S.; Shukla, A.K. Structural analysis of carbon nanospheres synthesized by CVD: An investigation of surface charges and its effect on the stability of carbon nanostructures. *Appl. Phys.* **2019**, *125*, 80, doi:10.1007/s00339-018-2372-0.